2001

Rotational spectroscopy of IO X2-pi-i

Charles E. Miller
Haverford College

Edward A. Cohen

Rotational spectroscopy of IO X2Πi

Charles E. Miller and Edward A. Cohen

Citation: J. Chem. Phys. **115**, 6459 (2001); doi: 10.1063/1.1398308
View online: http://dx.doi.org/10.1063/1.1398308
View Table of Contents: http://jcp.aip.org/resource/1/JCPSA6/v115/i14
Published by the American Institute of Physics.

Rotational spectroscopy of IO $X\,^2\Pi_i$

Charles E. Miller
Department of Chemistry, Haverford College, Haverford, Pennsylvania 19041-1392

Edward A. Cohen
Jet Propulsion Laboratory, California Institute of Technology, Pasadena, California 91109-8099

(Received 5 June 2001; accepted 10 July 2001)

Pure rotational spectra of the IO radical have been observed for vibrational levels up to $v=13$ in the $X_1\ ^2\Pi_{3/2}$ state and up to $v=9$ in the $X_2\ ^2\Pi_{1/2}$ state. Isotopically enriched $I^{18}O$ rotational spectra have been observed for vibrational levels up to $v=5$ in both the X_1 and X_2 states. These are the first high-resolution spectra of any kind reported for the X_2 state and greatly extend the available data for the X_1 state. The data for both isotopomers have been fitted simultaneously to a single set of $^2\Pi$ parameters with fixed isotopic ratios. The isotope relations among the parameters have provided a means of decorrelating the electron spin-rotation constant γ from the fine-structure centrifugal distortion constant, A_D, and have allowed the first determination of an effective value for γ. The rotation–vibration constants correspond to the equilibrium molecular properties $r_e(X_1)=186.762$ pm, $r_e(X_2)=188.468$ pm, $\omega_e(X_1)=681.69$ cm^{-1}, and $\omega_e(X_2)=645.29$ cm^{-1}. These constants have been used to calculate X_1 and X_2 Rydberg–Klein–Rees potentials encompassing energies up to 40% of the dissociation limit. A complete set of hyperfine coupling constants has been determined for the first time and interpreted using appropriate relativistic atomic radial integrals. © *2001 American Institute of Physics.* [DOI: 10.1063/1.1398308]

INTRODUCTION

There has been considerable controversy over the impact of iodine oxides on atmospheric ozone depletion.[1,2] Chlorine and bromine oxides form photochemical cycles that destroy stratospheric ozone with alarming efficiency and catalytic cycles involving iodine oxides are even more efficient.[1] Solomon *et al.*[2] hypothesized that iodine oxides could cause substantial stratospheric ozone depletion even at total iodine concentrations as low as 1 part per trillion (ppt). Subsequent studies[3,4] concluded that the vertical transport rate of CH_3I, the dominant source of atmospheric iodine, was too slow to produce the required I_x concentrations in the stratosphere. However, recent atmospheric measurements have confirmed IO concentrations of 1–5 ppt in the upper troposphere and the marine boundary layer,[5,6] as well as concentrations in the 0.5–1.0 ppt level in the lower stratosphere.[7] As part of our continuing effort to provide accurate spectroscopic information for molecules of importance in atmospheric ozone depletion chemistry, we investigated the pure rotational spectrum of iodine monoxide (IO), the prototypical reactive iodine oxide.

The IO radical has proven difficult to study due to its rapid self-reaction. Much of the high-resolution spectroscopic information available for IO comes from studies of the strong $A_1\ ^2\Pi_{3/2} \leftarrow X_1\ ^2\Pi_{3/2}$ electronic transition. Durie and Ramsay[8] identified six vibronic levels of the $A_1 \leftarrow X_1$ absorption spectrum. Durie, Legay, and Ramsay[9] subsequently observed the $A_1 \rightarrow X_1$ system in emission and obtained rotational constants for the X_1 vibrational levels $v=0$-4, 6, and 9. Bekooy *et al.*[10] probed the (2-0), (2-1), and (2-2) vibronic bands of the $A_1 \leftarrow X_1$ system using microwave-optical double resonance spectroscopy. This study refined the rovibrational and Λ-doubling constants for the X_1 state and provided precise values for the quadrupole coupling constants and a partial set of magnetic hyperfine parameters. More recently, Wennberg *et al.*[4] reported rotationally resolved Fourier transform spectrum of the $A_1 \leftarrow X_1$ (2-0) band while Newman *et al.*[11] obtained cavity ringdown spectra for all six $(v'-0)$ bands of the $A_1 \leftarrow X_1$ spectrum.

There have also been a number of detailed spectroscopic investigations focused on the $X\ ^2\Pi$ state. Carrington *et al.*[12] and Brown *et al.*[13] reported ESR spectra of IO $X_1\ ^2\Pi_{3/2}$ in the $J=3/2$ and $J=5/2$ levels, respectively. These studies conclusively established the inversion of the IO $X\ ^2\Pi$ spin-orbit components. Byfleet *et al.*[14] determined the electric dipole moment. From the experimental g factors Brown *et al.*[13] estimated the fine-structure splitting to be $A_0 \approx -2330$ cm^{-1}. Saito[15] observed the $5/2 \leftarrow 3/2$ and $7/2 \leftarrow 5/2$ rotational transitions of the X_1 vibrational ground state using Stark modulated microwave spectroscopy. The precise rotational constant derived from this work was combined with the α_e value obtained from the emission spectrum[9] to calculate the $^2\Pi_{3/2}$ equilibrium bond length as $r_e=186.77(28)$ pm. Gilles *et al.*[16] reported a direct determination of the fine-structure interval $A_0=-2091(40)$ cm^{-1} and $\omega_e=758(25)$ cm^{-1} for the X_2 state from the photoelectron spectrum of IO^-. Franck–Condon simulations of the photoelectron spectrum were optimized with the $^2\Pi_{1/2}$ equilibrium bond length as $r_e=188.7(10)$ pm. Tamassia *et al.*[17] studied the X_2 (2-0) overtone band by laser magnetic resonance and reported the results of a combined analysis that incorporated data from Ref. 10.

Our preliminary investigations of the IO rotational spectrum probed the ground and two lowest excited vibrational

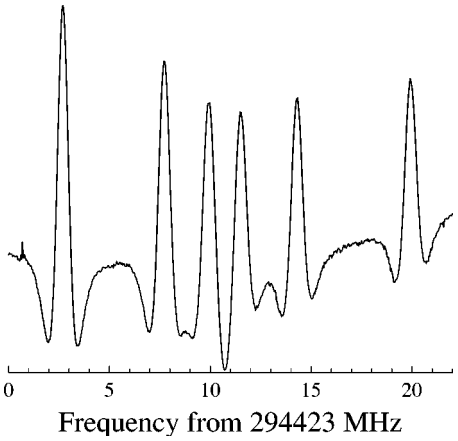

FIG. 1. The characteristic 1-4-1 hyperfine structure exhibited by IO $X_1\ ^2\Pi_{3/2}$ rotational transitions is shown here for the ($v=0$) 29/2←27/2 transition.

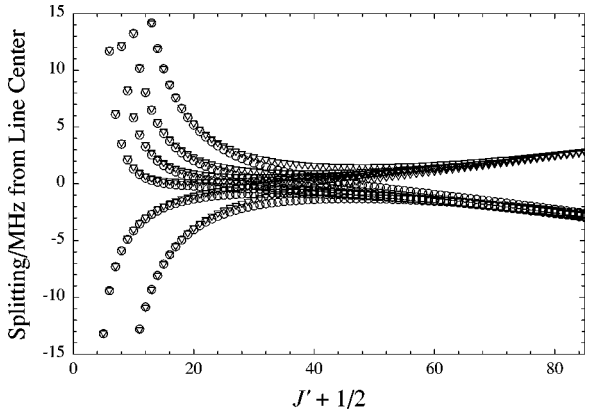

FIG. 2. The calculated hyperfine structure of the $X_1\ ^2\Pi_{3/2}\ v=0$ transitions plotted as a function of $J'+1/2$. Circles: e-parity Λ-doubling components. Inverted triangles: f-parity Λ-doubling components. See the text for additional details.

levels of the $X_1\ ^2\Pi_{3/2}$ state. While recording some weak $\Delta F=0$ transitions of the ground state, we observed a set of slightly stronger lines with a hyperfine pattern similar to that of the strong $\Delta F=1$ transitions. Calculations showed that the new lines belonged to X_1 rotational transitions of the $v=8$ level. Optimization of the IO source chemistry enabled us to observe pure rotational transitions of IO in vibrational levels of the $X_1\ ^2\Pi_{3/2}$ and $X_2\ ^2\Pi_{1/2}$ states with up to 8000 cm^{-1} of total energy. The extensive number of precise transition frequencies measured in this study has enabled us to derive accurate equilibrium spectroscopic constants and Rydberg–Klein–Rees (RKR) potentials for both $^2\Pi$ states. We also report the first complete set of hyperfine constants and discuss their values in terms of relativistic contributions to the electronic structure of the IO radical.

RESULTS

The submillimeter spectrometer used in these experiments has been described previously.[18,19] Measurements were made using a 1-m long double-pass absorption cell with a Zeeman coil wrapped around its entire length. Spectra were observed at room temperature in selected regions between 51 and 679 GHz. The submillimeter radiation was detected by a liquid-helium-cooled InSb hot electron bolometer, digitized, and recorded by a personal computer.

IO radicals were initially generated by flowing the products of an O_2 discharge over a sample of iodine crystals contained in an open ended pyrex tube that had been placed in the bottom of the absorption cell. Optimal IO production was achieved at the maximum available pumping speed (24 l/sec) with the O_2 flow rate adjusted to maintain pressures in the 85–100-mtorr range. The reaction was accompanied by a bright chemiluminescence which served as an excellent diagnostic of successful IO production.

Figure 1 displays an example of a typical $X_1\ ^2\Pi_{3/2}$ rotational transition. The sextet hyperfine structure (hfs) associated with the ^{127}I nuclear spin (I = 5/2) appears in a characteristic 1-4-1 splitting pattern in this frequency range. Figure 2 depicts the calculated $^2\Pi_{3/2}$ hyperfine splitting as a function of J. For low-J values each feature is an unresolved Λ doublet. The four central hfs components are resolved for low to moderate J transitions but coalesce as J increases beyond 35/2. Near $J=55/2$ the Λ doubling and hyperfine splittings are on the order of 0.5 MHz and the 12 line pattern is severely blended. At the high-J limit Λ doubling dominates, the transitions group by parity, and the pattern transforms into a doublet of unresolved sextets.

Eventually X_1 transitions associated with vibrational levels up to $v=12$ were observed with this source chemistry. Although no experiments have been performed in this study to determine the IO excitation mechanism, we note that the X_1 ($v=12$) level of IO contains approximately 7480 cm^{-1} of

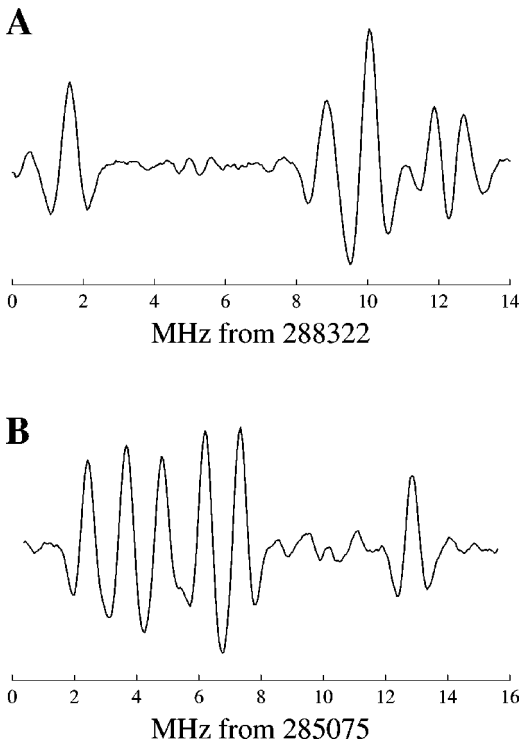

FIG. 3. Characteristic hyperfine patterns for the IO $X_2\ ^2\Pi_{1/2}$ state illustrated with the ($v=1$) 31/2←29/2 transition. (**A**) Upper Λ-doubling component showing 1-5 splitting. (**B**) Lower Λ-doubling component showing 5-1 splitting.

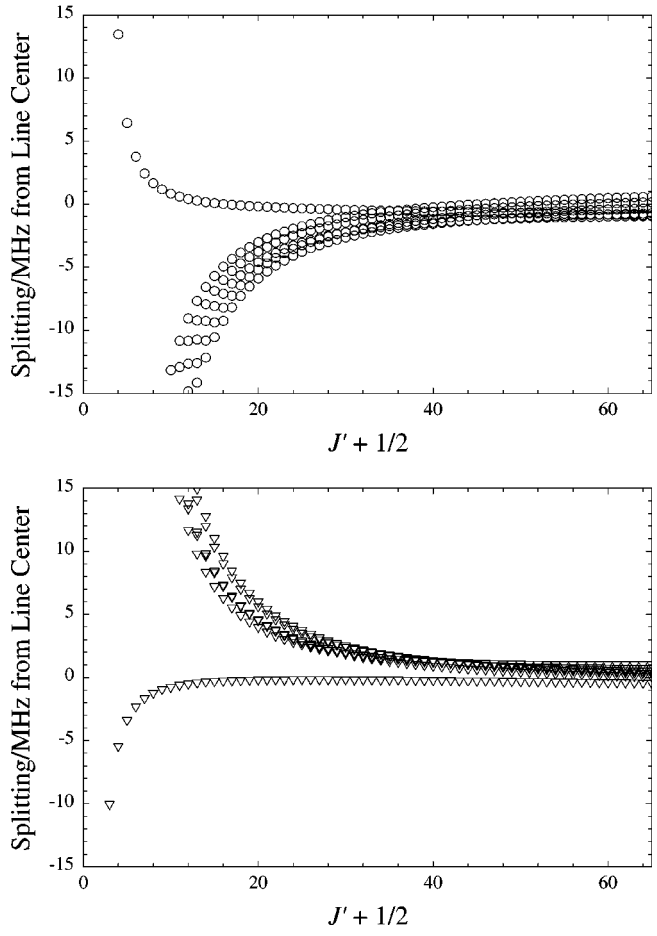

FIG. 4. The hyperfine structure of the $X_2\ ^2\Pi_{1/2}\ v=0$ transitions plotted as a function of $J'+1/2$. Circles: e-parity Λ-doubling components; inverted triangles: f-parity Λ-doubling components. The Λ doublets are separated by approximately 3.62 GHz.

vibrational excitation. This is comparable to the 7918 cm^{-1} of electronic energy contained in $O_2(a\ ^1\Delta_g)$ as well as the 7603 cm^{-1} of electronic energy in I* $(5p^5\ ^2P_{1/2})$. Rotational transitions of $O_2(a\ ^1\Delta_g)$ were readily observed in the reaction mixture. We suspect that the reaction mixture also contained a significant concentration of I* since the rapid, efficient energy transfer between $O_2(a\ ^1\Delta_g)$ and I to form I* is well known.

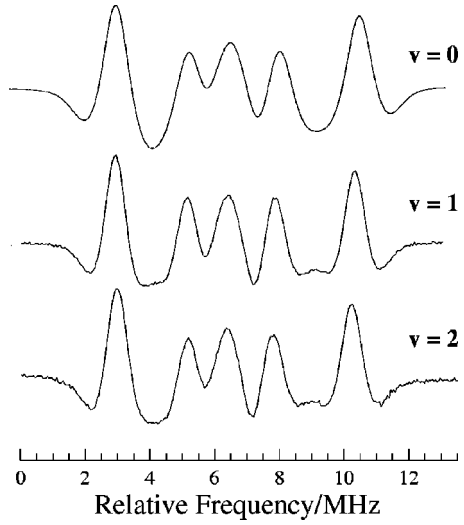

FIG. 5. $I^{18}O$ rotational transitions for $X_1\ ^2\Pi_{3/2}$ showing the vibrational state dependence of the hyperfine structure.

TABLE I. Distribution of experimental uncertainties.

Uncertainty (kHz)	Number of features
6–25	179
26–50	249
51–100	102
101–150	62
151–300	29

No $X_2\ ^2\Pi_{1/2}$ rotational transitions were detected using the external microwave discharge source chemistry even though the 2091 cm^{-1} fine-structure splitting corresponds roughly to the $v=3$ level of X_1. However, when a 35 mA dc discharge was passed through the entire cell with 40 mTorr of O_2 flow, we observed significant enhancement of the high-v $^2\Pi_{3/2}$ transitions, X_1 $(v=13)$ transitions were observed for the first time, and prominent X_2 transitions from several vibrational levels were discovered. The X_2 rotational transitions were easily distinguished from X_1 transitions by their characteristic 1-5 or 5-1 hyperfine patterns, depending on whether the the transition belonged to the upper or lower Λ-doubling component (see Fig. 3). The J dependence of the X_2 hyperfine splitting patterns are shown in Fig. 4. Rotational transitions for X_2 vibrational levels $v=0-9$ are predicted within the spectral range scanned using the dc discharge source chemistry and transitions within all ten vibrational levels have been observed. A careful reexamination of the survey scans recorded using external microwave discharge source chemistry revealed some weak features at the correct frequencies for X_2 transitions, but these signals were far weaker than the features associated with X_1 transitions for states of similar internal energy. However, a later series of measurements in the 600-GHz region with an external microwave discharge did produce readily observable X_2 spectra. The reasons for the difference in behavior have not been determined.

Transition frequencies for $I^{18}O$ in both the X_1 and X_2 states were predicted using the isotopic dependencies of the spectroscopic constants (see below for details). These transitions were recorded using the dc discharge source chemistry and isotopically enriched $^{18}O_2$. Figure 5 presents a sample of the $I^{18}O$ spectra obtained under these conditions.

Iodine dioxide, OIO, was observed as an additional product of both IO source chemistries.[20] OIO was generated more efficiently in the dc discharge source although it did not interfere with the IO observations in either set of experiments. We note that anomalous vibrational excitation was not apparent in OIO.

A total of 615 features in the 50–680 GHz region as well as the six $\Delta J=0$, Λ-doubling transitions measured by Bekooy *et al.*[10] are included in the fit. These correspond to 1293 assignments of individual transitions. Of the fitted features 211 were single lines and 354 were unresolved pairs of lines, usually Λ doublets. Experimental uncertainties ranged

TABLE II. The IO $X\ ^2\Pi$ v and J states spanned by the data set.

v	$X_1\ ^2\Pi_{3/2}$	$X_2\ ^2\Pi_{1/2}$
	$^{127}I^{16}O$	
0	$5/2 \leqslant J \leqslant 65/2$	$3/2 \leqslant J \leqslant 63/2$
1	$5/2 \leqslant J \leqslant 65/2$	$5/2 \leqslant J \leqslant 43/2$
2	$5/2 \leqslant J \leqslant 65/2$	$5/2 \leqslant J \leqslant 43/2$
3	$5/2 \leqslant J \leqslant 65/2$	$27/2 \leqslant J \leqslant 43/2$
4	$7/2 \leqslant J \leqslant 65/2$	$31/2 \leqslant J \leqslant 63/2$
5	$27/2 \leqslant J \leqslant 65/2$	$31/2 \leqslant J \leqslant 43/2$
6	$27/2 \leqslant J \leqslant 67/2$	$41/2 \leqslant J \leqslant 45/2$
7	$27/2 \leqslant J \leqslant 67/2$	$29/2 \leqslant J \leqslant 45/2$
8	$27/2 \leqslant J \leqslant 67/2$	$29/2 \leqslant J \leqslant 57/2$
9	$29/2 \leqslant J \leqslant 67/2$	$43/2 \leqslant J \leqslant 45/2$
10	$29/2 \leqslant J \leqslant 65/2$	
11	$29/2 \leqslant J \leqslant 45/2$	
12	$39/2 \leqslant J \leqslant 45/2$	
13	$33/2 \leqslant J \leqslant 47/2$	
	$^{127}I^{18}O$	
0	31/2, 33/2, 41/2, 43/2	45/2, 47/2
1	31/2, 33/2, 41/2, 43/2	45/2, 47/2
2	31/2, 33/2, 41/2, 43/2	
3	31/2, 33/2, 41/2, 43/2	
4	31/2, 33/2, 41/2, 43/2	
5	41/2, 43/2	47/2, 49/2

from 6 to 30 kHz for the six transitions from Refs. 10 and 15 to 300 kHz for the newly measured features. The distribution of the experimental uncertainties is shown in Table I. Table II summarizes the quantum states spanned by the data and Fig. 6 shows the distribution of the measurements among the electronic states and isotopes. All fits were made with Pickett's SPFIT program,[21] which weights data inversely as the square of the uncertainty. The reduced rms was 0.78 corresponding to an overall rms of 53 kHz. Data included in the fit were all within 2.5 times their uncertainty from the calculated frequencies. These are the first high-resolution measurements of the X_2 state and the ^{18}O isotopomer. Files containing the complete line list with observed and calculated line positions, the optimized fitting parameters, and the correlation coefficient matrix have been deposited with the journal.[22]

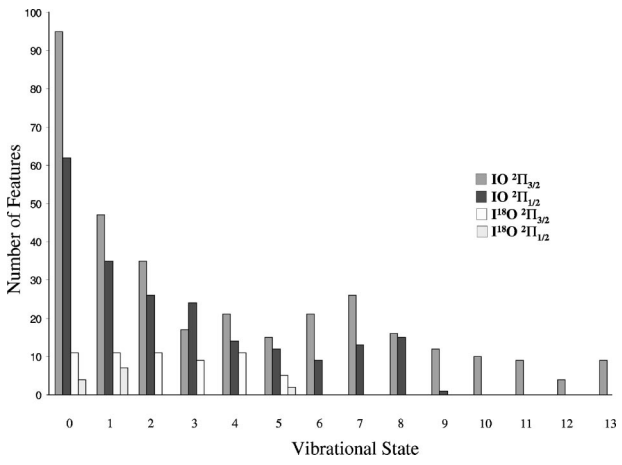

FIG. 6. Number of features included in the fit.

DISCUSSION

The present study provides the first high-resolution characterization of the IO $X\ ^2\Pi$ state to include transitions from both spin-orbit components. We have determined a set of isotopically independent spectroscopic parameters by simultaneously fitting $^{127}I^{16}O$ and $^{127}I^{18}O$ transitions for the $X_1\ ^2\Pi_{3/2}$ state in vibrational levels up to $v=13$ and $X_2\ ^2\Pi_{1/2}$ state in vibrational levels up to $v=9$. These parameters describe the equilibrium values, vibrational dependencies and centrifugal distortion of the mechanical, Λ doubling, and hfs constants. The inclusion of two isotopomers in the fit has enabled the first determination of the electron spin-rotation constant γ as well as the deviations of the constants Y_{01} and Y_{11} from the Born–Oppenheimer approximation.

The following analysis mirrors that presented in our recent report of the BrO rotational spectrum.[19] The BrO data were analyzed first since the new submillimeter transitions could be merged with existing microwave data, experimental measurements of the BrO $X_2\ ^2\Pi_{1/2} \leftarrow X_1\ ^2\Pi_{3/2}$ fine-structure transition and rotationally resolved infrared spectra. The experience gained from fitting the comprehensive BrO data set led to a method for fitting spectra of multiple isotopomers simultaneously using the effective $^2\Pi$ Hamiltonian of Brown *et al.*[23] The vibrational, centrifugal distortion, and isotope dependencies of all mechanical, fine-structure, and hyperfine-structure parameters have been defined in the operator language of SPFIT[21] and systematically applied to the $X\ ^2\Pi$ spectra of the entire halogen monoxide series,[19,24,25] culminating with the present analysis of IO. Readers interested in the specific form of the Hamiltonian should consult Refs. 19 and 24.

Rovibrational constants, fine-structure constants, and interatomic potentials

The optimized rovibrational and fine structure constants determined in the final fit are reported in Table III. The atomic masses used to determine the reduced mass ratios were taken from Audi and Wapstra.[26] The uncertainties reported are approximately 1σ and do not include contributions from the uncertainty in A. For the equilibrium parameters, these reflect correlations with the higher-order constants which describe the vibrational dependence. The combinations of parameters that determine the rotational transition frequencies for the lower vibrational levels, particularly those of the X_1 state, are considerably more precise. These may be generated from the files of extended precision parameters and correlation coefficients which have been deposited with the journal.[22] Calculated spectra based on these parameters have been placed in the JPL *Submillimeter, Millimeter, and Microwave Spectral Line Catalog*.[27]

TABLE III. IO $X\ ^2\Pi$ mechanical parameters in MHz. Fit with the ground state $A=-2091\ \mathrm{cm}^{-1}$ (Ref. 16) and the $A_{l,0}$ values in Table IV. The numbers in parentheses are 1σ uncertainties in units of the last digit.

Parameter	Value	Isotope dependence
A_{01}	183.8439(65)	μ^{-1}
A_{11}	2.8719(12)	$\mu^{-3/2}$
$A_{21}\times10^3$	−17.55(54)	μ^{-2}
$A_{31}\times10^3$	1.085(93)	$\mu^{-5/2}$
$A_{41}\times10^6$	60.6(53)	μ^{-3}
$A_{02}\times10^3$	0.576 77(84)	μ^{-2}
$A_{12}\times10^6$	1.88(66)	$\mu^{-5/2}$
$A_{22}\times10^6$	0.802(83)	μ^{-3}
Y_{01}	10107.594 34(44)	μ^{-1}
δ_{01}^{O}	0.7672(31)	$\mu^{-1}M_{\mathrm{O}}^{-1}$
Y_{11}	−82.635 26(62)	$\mu^{-3/2}$
$\delta_{11}^{\mathrm{O}}\times10^3$	−7.36(72)	$\mu^{-3/2}M_{\mathrm{O}}^{-1}$
Y_{21}	−0.129 84(30)	μ^{-2}
$Y_{31}\times10^3$	−9.491(54)	$\mu^{-5/2}$
$Y_{41}\times10^3$	−0.1019(40)	μ^{-3}
$Y_{51}\times10^6$	−6.20(11)	$\mu^{-7/2}$
Y_{02}	−0.010 451 62(66)	μ^{-2}
$Y_{12}\times10^3$	−0.06122(42)	$\mu^{-5/2}$
$Y_{22}\times10^6$	−2.476(82)	μ^{-3}
$Y_{32}\times10^6$	−0.1655(50)	$\mu^{-7/2}$
$Y_{03}\times10^9$	−7.24(38)	μ^{-3}
$Y_{13}\times10^9$	−0.640(92)	$\mu^{-7/2}$
γ [a]	−799.0(19)	μ^{-1}
p_{00}	3280.366(76)	μ^{-1}
p_{10}	−13.801(15)	$\mu^{-3/2}$
p_{20}	−0.2842(48)	μ^{-2}
$p_{30}\times10^3$	6.02(39)	$\mu^{-5/2}$
$p_{01}\times10^3$	−0.266(24)	μ^{-2}
$p_{11}\times10^3$	−0.3711(93)	$\mu^{-5/2}$
q	−0.499(37)	μ^{-2}

[a]The variation of γ with A, $\partial\gamma/\partial A\approx5.06\ \mathrm{MHz/cm}^{-1}$.

The parameters include the deviations from the Born–Oppenheimer approximation $\delta_{01}^{\mathrm{O}}=0.7672(31)$ MHz and $\delta_{11}^{\mathrm{O}}=-7.36(72)$ kHz. Le Roy[28] has defined isotope dependent quantities, $\delta_{l,n}^{\mathrm{A}}$, such that for a halogen oxide XO we have

$$Y_{l,n}=\mu^{-(l+2n)/2}U_{l,n}-\delta_{l,n}^{\mathrm{O}}-\delta_{l,n}^{\mathrm{X}}. \tag{1}$$

The oxygen correction is of the order magnitude indicated by Watson[29] with the relation

$$\delta_{l,n}^{\mathrm{O}}=-U_{l,n}\Delta_{l,n}^{\mathrm{O}}m_e/(\mu M_{\mathrm{O}}). \tag{2}$$

We note that for ClO, BrO, and IO, $\Delta_{01}^{\mathrm{O}}=-2.240(13)$, −1.963(4), and −2.213(9), respectively. Since there is only one iodine isotope, only the oxygen correction is determinable. For ClO and BrO $\Delta_{01}^{\mathrm{X}}=-1.419(24)$ and −1.124(48). If $\Delta_{01}^{\mathrm{I}}\approx-1$, we estimate $\delta_{01}^{\mathrm{I}}\approx44$ kHz. This is only a minor part of the total correction and the quantity $Y_{l,n}+\delta_{l,n}^{\mathrm{I}}$ has been used to approximate $\mu^{-(l+2n)/2}U_{l,n}$ for Y_{10} and Y_{11}.

One may recover Dunham parameters for the X_1 and X_2 states from the fitted $Y_{l,n}$ and the fine-structure constants $A_{l,n}$ via the relationship

$$Y_{l,n}^{*}=Y_{l,n}\pm A_{l,n}/2 \tag{3}$$

where the sum in Eq. (3) refers to the $X_1\ ^2\Pi_{3/2}$ state and the difference refers to the $X_2\ ^2\Pi_{1/2}$ state.[30] The $Y_{l,n}^{*}$ can be used to derive Dunham potential coefficients[31,32] for the X_1 and X_2 states using the expansion

$$V(\xi)=a_0\xi^2\left(1+\sum_{i\geqslant1}a_i\xi^i\right) \tag{4}$$

where $\xi=(r-r_e)/r_e$. Even though there are no vibrational energy intervals explicitly included in the IO data, the parameter set includes extensive information on the vibrational dependence of the rotational constants. The a_i^{*}'s derived from the data contain sufficient information to calculate the pure vibrational terms $Y_{l,0}^{*}$ and the vibrational energies for X_1 and X_2. Equation (5) shows that the $Y_{l,0}^{*}$ lead immediately to the vibrational state dependence of the fine-structure interval

$$\begin{aligned}A_{l,0}&=Y_{l,0}^{*}(^2\Pi_{3/2})-Y_{l,0}^{*}(^2\Pi_{1/2}),\\ A_{00}&=A_e+Y_{00}^{*}(^2\Pi_{3/2})-Y_{00}^{*}(^2\Pi_{1/2}).\end{aligned} \tag{5}$$

where $A(r)=V_{X_2}(r)-V_{X_1}(r)$ decreases almost linearly from 2600 cm^{-1} at $r=165.0$ pm to 795 cm^{-1} at $r=240.0$ pm.

The calculated Dunham potential coefficients, a_1, $Y_{l,0}^{*}$, $A_{l,0}$, and equilibrium bond lengths for the $X_1\ ^2\Pi_{3/2}$, $X_2\ ^2\Pi_{1/2}$, and average $X\ ^2\Pi_{\mathrm{eff}}$ states are presented in Table IV. Uncertainties have not been propagated for the values in Table IV, but the number of significant figures given enables one to reproduce the observed constants within experimental uncertainty.

Table V shows the X_1 vibrational term values derived from the parameters in Table IV. For comparison, the experimental[9–11] values and those calculated from a three-term fit ($Y_{10}=681.4683\ \mathrm{cm}^{-1}$, $Y_{20}=-4.295\,94\ \mathrm{cm}^{-1}$, and $Y_{30}=-0.012\,80\ \mathrm{cm}^{-1}$) which reproduced the observed X_1 values with an rms error of 0.03 cm^{-1} are also shown. We note that the two sets of calculated vibrational origins never deviate by more than 1.5 cm^{-1} from each other. This provides some confidence that the calculated X_2 vibrational levels are of comparable accuracy. Figure 7 shows the RKR potentials and vibrational energy manifolds derived from the parameters of Tables III and IV. The RKR turning points and energy for each state are given in Table VI. These have been calculated using a program obtained from Le Roy[33] and $Y_{l,0}$ and $Y_{l,1}$ values that were derived from only rotational data.

Note that the energy differences between the X_2, v and $X_1, v+3$ states are quite small and decrease with increasing v. Since the reported[16] uncertainty of A is 40 cm^{-1} and the calculated differences range from 98 to 14 cm^{-1} for the observed states, the possibility of a resonant interaction cannot be ruled out. However, no clear evidence of such an interaction is apparent in the data set. We estimate the main contribution to the matrix element (case a basis) between the states

$$\begin{aligned}&\langle X_1, v+3|\mathcal{H}|X_2, v\rangle\\ &\quad\approx-4\left(\frac{B^3(v+1)(v+2)(v+3)}{\omega^3}\right)^{1/2}\langle X_1, v|\mathcal{H}|X_2, v\rangle.\end{aligned} \tag{6}$$

TABLE IV. IO potential constants and derived parameters.

Parameter	$X_1\ ^2\Pi_{3/2}$	$X_2\ ^2\Pi_{1/2}$	$X\ ^2\Pi_{\text{eff}}$
a_0 (cm^{-1})	341 528.83	311 640.68	326 145.39
a_1	−3.658 74	−3.702 29	−3.680 27
a_2	8.205 60	8.527 59	8.365 43
a_3	−15.249 02	−16.508 05	−15.869 30
a_4	25.007 00	26.545 23	25.631 93
a_5	−60.015 87	−42.914 09	−50.255 88
a_6	189.076 03	64.792 47	121.200 85
Y_{00} (cm^{-1})	0.050 64	0.066 64	0.058 74
Y_{10} (cm^{-1})	681.772 45	645.362 03	663.232 27
Y_{20} (cm^{-1})	−4.352 11	−4.313 10	−4.331 91
Y_{30} (cm^{-1})	−0.003 75	−0.004 85	−0.004 36
Y_{40} (cm^{-1})	−0.000 50	−0.000 45	−0.000 48
A_{10} (cm^{-1})			36.410 43
A_{20} (cm^{-1})			−0.039 00
A_{30} (cm^{-1})			0.001 10
A_{40} (cm^{-1})			−0.000 04
r_e (pm) [a]	186.761 88(2)	188.468 02(6)	187.609 13(3)

[a]The r_e uncertainties reflect only 1σ experimental uncertainties. The Born–Oppenheimer correction for the I atom is neglected in the calculation, but may add ≈0.0004 pm to the tabulated values.

Only contributions from the rotational constant are considered in the above expression. Only in the case of interacting states separated by energies of the order of a rotational constant will the perturbations be appreciable compared to the normal vibration–rotation interaction terms. If such resonances exist for accessible energy levels, a more precise determination of A will be necessary to search for the effects in the rotational spectrum. Introducing a fixed term given by Eq. (6) into the fit produced only changes of the order of 0.01σ in even the smallest parameters and the effects were not considered further.

The results summarized in Table IV indicate that there are significant physical differences between the X_1 and X_2 states. Most notably, the isotopically independent equilibrium bond length increases from 186.761 88(2) pm in the X_1 state to 188.468 02(6) pm in the X_2 state. The $\Delta r = 1.706\ 14$ pm change between the two spin-orbit states is comparable to the bond length changes usually associated with electronic transitions. The change in harmonic vibrational frequencies, $\Delta Y_{10}^* = -36.4\ \text{cm}^{-1}$, is also substantial; for comparison, it is a factor of 2 larger than the $\Delta Y_{10}^* = -14.9\ \text{cm}^{-1}$ observed for BrO.[19] These changes indicate a weakening of the I–O bond in the X_2 state.

Figure 8 compares the X_1 and X_2 RKR potentials with the *ab initio* potentials of Roszak *et al.*[34] calculated at the multireference single- and double-excitation configuration interaction level of theory. The *ab initio* calculations include spin-orbit coupling and employed relativistic effective core potentials for the iodine atom. The *ab initio* calculations systematically overestimate the I–O internuclear separation due to the freezing of the iodine 4*d* electrons at the configuration interaction step.[34] The fairly diffuse 4*d* electrons of the iodine atom are significantly polarized by the strongly electronegative oxygen atom.[34] This leads to stronger bonding, $r_e^{\text{expt}}(X_1) = 186.762$ pm versus $r_e^{\text{theor}}(X_1) = 192.2$ pm and $r_e^{\text{expt}}(X_2) = 188.468$ pm versus $r_e^{\text{theor}}(X_2) = 193.9$ pm, and larger vibrational frequencies, $\omega_e^{\text{expt}}(X_1) = 681.7\ \text{cm}^{-1}$ ver-

TABLE V. $I^{16}O\ X_1\ ^2\Pi_{3/2}$ vibrational intervals $E(v) - E(0)$.

v	From fit to intervals	Observed	From derived potential
1	672.83	672.8607[a]	673.05
2	1336.96	1336.9816[a]	1337.35
3	1992.31	1992.35[b]	1992.85
4	2638.79	2638.73[b]	2639.50
5	3276.34		3277.21
6	3904.87	3904.88[b]	3905.92
7	4524.31		4525.52
8	5134.58		5135.92
9	5735.61	5735.61[c]	5736.98
10	6327.32		6328.58

[a]Calculated from the band origins reported in Ref. 10.
[b]Calculated from the band origins reported in Refs. 9, 11.
[c]Calculated from the band origins reported in Ref. 9.

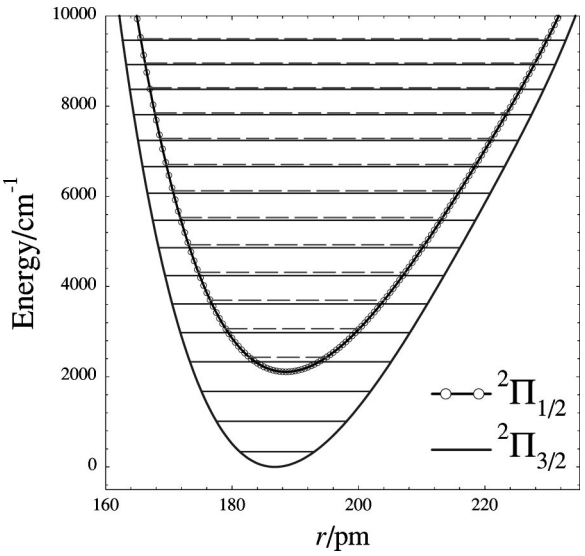

FIG. 7. The IO $X_1\ ^2\Pi_{3/2}$ (solid line) and $X_2\ ^2\Pi_{1/2}$ (open circles) RKR potentials and vibrational manifolds derived from the fitted spectrum.

TABLE VI. RKR Turning points for the $I^{16}O$ $X\ ^2\Pi$ Potentials. Energies in cm^{-1}; bond lengths in pm.

	$X_1\ ^2\Pi_{3/2}$			$X_2\ ^2\Pi_{1/2}$		
v	Energy	r_{min}	r_{max}	Energy[a]	r_{min}	r_{max}
0	339.85	181.19	193.02	2430.85	182.75	194.91
1	1012.90	177.49	198.10	3067.57	178.96	200.16
2	1677.20	175.12	201.87	3695.60	176.54	204.06
3	2332.73	173.29	205.11	4314.90	174.68	207.43
4	2979.35	171.78	208.07	4925.41	173.14	210.49
5	3617.07	170.48	210.83	5527.05	171.83	213.36
6	4245.77	169.33	213.46	6119.74	170.66	216.10
7	4865.38	168.30	216.00	6703.38	169.62	218.75
8	5475.76	167.38	218.46	7277.88	168.68	221.32
9	6076.82	166.53	220.87	7843.10	167.82	223.84
10	6668.42	165.74	223.25	8398.94	167.03	226.33
11	7250.42	165.02	225.60	8945.26	166.30	228.79
12	7822.66	164.34	227.93	9481.89	165.61	231.24
13	8384.97	163.70	230.27			
14	8937.19	163.11	232.60			
15	9479.10	162.55	234.93			

[a]Adjusted so that $A_0 = -2091\ cm^{-1}$.

sus $\omega_e^{theor}(X_1) = 650\ cm^{-1}$ and $\omega_e^{expt}(X_2) = 645.3\ cm^{-1}$ versus $\omega_e^{theor}(X_2) = 626\ cm^{-1}$, in the experimental values. The *ab initio* $V_{X_1}(r)$ and $V_{X_2}(r)$ have therefore been reduced by 5.0 pm to create Fig. 8. We note that the relative precision of the *ab initio* calculations is much better than their absolute accuracy, yielding $\Delta r_e^{theor} = 1.7$ pm and $\Delta\omega_e^{theor} = -24\ cm^{-1}$ compared to the values $\Delta r = 1.706$ pm and $\Delta Y_{10}^* = -36.4\ cm^{-1}$ derived from the fit. It is interesting to note that the *ab initio* calculations slightly overestimate the anharmonicity at large *r*. Alternatively, one may interpret this as an underestimation of the I–O bond strength in the attractive limb and once again attribute the deficiency to the fact that the effective core potentials fail to account for all of the polarization effects in the real molecule. Despite these shortcomings, the empirically corrected potentials of Roszak *et al.*[34] provide an excellent description for both the X_1 and X_2 states of the IO radical. It appears that future calculations employing full optimization of the iodine core electrons may be able to reproduce the IO potentials with near spectroscopic accuracy.

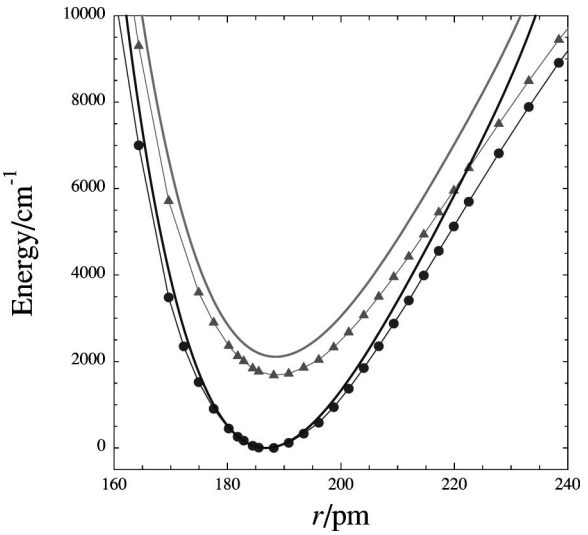

FIG. 8. A comparison of the IO $X_1\ ^2\Pi_{3/2}$ and $X_2\ ^2\Pi_{1/2}$ RKR (bold lines) and *ab initio* (filled symbols) potentials. The r_e values of the *ab initio* potentials (Ref. 34) have been reduced by 5.0 pm for better agreement with experiment. See text for additional details.

The effective parameters reported in this paper have been derived without explicit consideration of the difference in r_e between the X_1 and X_2 states. A more rigorous treatment would consider the less than unit overlap of the vibrational wave functions, $S_{v,v} = \langle X_1, v || X_2, v \rangle$. In the case of the halogen oxides, ignoring this effect results in no significant change to any molecular parameter, with the exception of the electron spin-rotation constant γ, which would affect its interpretation in terms of the interatomic potential or electron distribution. The fitting parameter γ listed in Table III actually represents an effective spin-rotation constant, as discussed by Brown *et al.*[23] It is an extremely difficult parameter to determine accurately since it is very sensitive to the value of the *A* and contributes primarily to the difference between the effective rotational constants of the X_1 and X_2 states. This is given to second order by

$$B(X_1) - B(X_2) = A_D + 2(B - \gamma/2)^2/(A - 2B). \tag{7}$$

The total contribution of the second term in Eq. (7) is slightly less than 2% that of $A_{01} \equiv A_{D_e}$ and that from γ is only 0.15% of A_{01}. For a single isotopic species, γ is entirely correlated with A_{01}. The correlation is removed by fitting the $^{127}I^{16}O$ and $^{127}I^{18}O$ spectra simultaneously with the assumption that γ and A_{01} vary exactly as μ^{-1}. The two terms in Eq. (7) have different isotope effects and can be separately determined. Since γ absorbs all contributions which make $\langle X_1, v | B - \gamma/2 | X_2, v \rangle$ different from *B*, it should be interpreted cautiously. Moreover, $\partial\gamma/\partial A \approx 5.06$ MHz/cm^{-1} and the uncertainty of *A* is 40 cm^{-1}.

The effect of the vibrational overlap on γ is a significant fraction of its fitted value. For $I^{16}O$ and $I^{18}O$ $\langle X_1, v || X_2, v \rangle = 0.97887$ and 0.97781, respectively. Unlike the lighter halogen oxides, the difference in overlap between the two iso-

TABLE VII. Comparison of the halogen monoxide and nitrogen monohalide electron spin-rotation constants.

	XO			NX	
X	γ^*	γ^*/B	$-p_{00}/2$	γ	γ/B
Cl	−300[a]	−0.0160	−339.3	−208.6[b]	−0.0108
Br	−760[c]	−0.0592	−913.9	−517.1 [d]	−0.0386
I	−1043[e]	−0.1032	−1640.2	−640.2[f]	−0.0620

[a]Reference 24, γ and p_{00} in MHz.
[b]Reference 35.
[c]Reference 19.
[d]Reference 36.
[e]This work.
[f]Reference 37.

topes is also important in determining the value of γ^* for unit overlap. To second order

$$(2B-\gamma)_{\text{fit}}=\left(\frac{S_{0,0}^2(\mathrm{I}^{16}\mathrm{O})-\rho S_{0,0}^2(\mathrm{I}^{18}\mathrm{O})}{1-\rho}\right)^{1/2}(2B-\gamma^*), \tag{8}$$

where ρ is the ratio of the reduced mass of $I^{16}O$ to that of $I^{18}O$. When the isotopic difference in overlap is very small, this expression reduces to Eq. (11) of Ref. 19. The result is that $\gamma^*\approx -1043$ MHz, which is considerably larger that the fitted value of -799 MHz. The values of γ^* for the halogen oxides are compared with γ for the corresponding nitrogen monohalides in Table VII. It can be seen that the trends across both series are similar with the oxide values being about 50% higher throughout. The value of γ as discussed below is roughly proportional to both the rotational constant and the effective electron spin-orbit coupling constant A. A is often estimated for a diatomic molecule by the spin density weighted sum of the atomic spin-orbit couplings. This has been done for the NX series[35–37] with A calculated to be about half the value of the corresponding oxide. Thus, in spite of the difficulties in determining accurate values of γ for the $^2\Pi$ series of XO molecules, the results appear consistent with those obtained for the NX $^3\Sigma$ series for which the determination is more direct and precise. Since the fitted value of γ depends strongly on the fixed value of A, the consistency of the results as well as good agreement of other IO and BrO parameters determined by photoelectron spectroscopy[38] suggests that A lies within the limits given by Gilles *et al.*[16]

The $X\ ^2\Pi$ Λ-doubling constants p and q, as well as the spin-rotation constant γ^* may be used to deduce information on low-lying excited states. For $^2\Pi$ states, it is often assumed that the main contributions to these terms arise from perturbations by nearby $^2\Sigma$ states. The second-order expressions for these constants are[39]

$$p=-2\sum_i \pm\frac{\langle^2\Pi|L_+A|^2\Sigma^\pm\rangle\langle^2\Sigma^\pm|L_-B|^2\Pi\rangle}{\Delta E_i}, \tag{9}$$

$$q=-2\sum_i \pm\frac{\langle^2\Pi|L_+B|^2\Sigma^\pm\rangle^2}{\Delta E_i}, \tag{10}$$

$$\gamma^{(2)}=\sum_i \frac{\langle^2\Pi|L_+A|^2\Sigma^\pm\rangle\langle^2\Sigma^\pm|L_-B|^2\Pi\rangle}{\Delta E_i}, \tag{11}$$

where $\gamma^*=\gamma^{(1)}+\gamma^{(2)}$ and $\gamma^{(2)}$ is the dominant contribution. Equations (9) and (10) imply that $p/q\approx A/B$. For $^{127}I^{16}O$, $p/q=-6534(2)$ and $A/B=-6255$, which suggests that the single perturber approximation is fairly good for the $X\ ^2\Pi_i$ state. The positive value of p obtained from the fit implies that Σ^+ states dominate the sum in Eq. (9). It also implies that $\gamma\approx -p/2$. Table VII shows that this last relationship holds quite well for ClO, but worsens progressively for the heavier halogens. Contrary to the relation between p and q, this suggests that the $X\ ^2\Pi$ mixing with low-lying electronic states becomes more complex with increasing molecular weight and increasing magnitude of the spin-orbit coupling constant.

If one assumes that a single $^2\Sigma^+$ state is responsible for the observed Λ doubling in $X\ ^2\Pi$, then the perturbing state is located near 25 800 cm^{-1} or 27 200 cm^{-1} depending on whether one calculates the $^2\Sigma^+-X^2\Pi$ energy difference using the fit value of p or q. These results are consistent with the observed energy of the $A_1\ ^2\Pi_{3/2}\leftarrow X_1\ ^2\Pi_{3/2}$ electronic transition, which is predissociated by crossings with multiple repulsive states.[11] Calculations of the $^2\Sigma^+-X^2\Pi$ energy differences for BrO (Ref. 19) and ClO (Ref. 24) yielded similar results. The IO calculations are also consistent with the excitation energies of 23 200 cm^{-1} ($1\ ^2\Sigma^-$), 23 900 cm^{-1} ($1\ ^2\Sigma^+$), and 26 250 cm^{-1} ($2\ ^2\Sigma^-$) predicted by Roszak *et al.* in the L-S coupling limit.[34] Note, however, that *ab initio* calculations implemented in the spin-orbit coupling limit[34] predict six electronic states with $\Omega=\frac{1}{2},\frac{3}{2}$ between 23 700 and 29 800 cm^{-1}.

Hyperfine constants

The extensive set of $X_1\ ^2\Pi_{3/2}$ and $X_2\ ^2\Pi_{1/2}$ submillimeter transitions measured in this work enabled us to determine the first complete set of hfs constants for IO. The optimized values of the nuclear spin-rotation constant C_I and the magnetic hyperfine constants a, b_F, c, and d are given in Table VIII. The table also contains the linear combinations of constants $b_{00}=b_F-c_{00}/3$, and $h_{\pm_{00}}=a_{00}\pm\frac{1}{2}(b_{00}+c_{00})$. The parameter h_+ is considerably better known than is apparent from the uncertainties of the individual fitted constants due to correlations among them. This reflects the more extensive and precise data available for the X_1 state. The hfs patterns, illustrated in Figs. 1 and 4, were measured with sufficient precision that the fit yielded linear vibrational dependencies for a, the sum $(b+c)$, and d. Centrifugal distortion of d was also required to fit the spectrum. The centrifugal distortions of the other primary magnetic constants cannot be reliably determined since they are strongly correlated with C_I and b_F and cannot be decorrelated by their isotope effects. The nonaxial nuclear spin-rotation constant, C_I', does not affect the quality of the fit, has a 1σ uncertainty that is slightly larger than its magnitude, and has been excluded from the final parameter set.

The definitions of the magnetic hyperfine and quadrupole coupling constants

TABLE VIII. IO $X\ ^2\Pi$ hyperfine parameters in MHz. The numbers in parentheses are 1 σ uncertainties in units of the last digit.

Parameter	Value	Isotope dependence
a_{00}	774.824(92)	g_N
a_{10}	−14.27(12)	$g_N\mu^{-1/2}$
b_F	−95.8(37)	g_N
c_{00}	−416.7(56)	g_N
$(b_F+\frac{2}{3}c)_{10}$	12.16(23)	$g_N\mu^{-1/2}$
d_{00}	1119.650(82)	g_N
d_{10}	−23.00(15)	$g_N\mu^{-1/2}$
$d_{01}\times10^3$	−4.536(15)	$g_N\mu^{-1}$
C_I	0.077 41(94)	$g_N\mu^{-1}$
$h_{+_{00}}$	588.042(16)	g_N
$h_{-_{00}}$	961.61(18)	g_N
b_{00}	43.1(56)	g_N
$eQq_{1_{00}}$	−1986.90(33)	Q
$eQq_{1_{10}}$	−17.27(49)	$Q\mu^{-1/2}$
$eQq_{1_{01}}\times10^3$	−4.55(31)	$Q\mu^{-1}$
$eQq_{S_{00}}$	198.17(65)	Q
$eQq_{S_{10}}$	1.13(49)	$Q\mu^{-1/2}$
eQq_2	−3111.0(19)	Q
$eQq_{1_{00}}(X_1)$	−1887.82(14)	Q
$eQq_{1_{00}}(X_2)$	−2085.98(63)	Q

$$
\begin{aligned}
a &= 2g_N\mu_e\mu_N\langle 1/r^3\rangle_L,\\
b_F &= (8\pi/3)g_eg_N\mu_e\mu_N\langle\psi^2(0)\rangle_S,\\
c &= (3/2)g_eg_N\mu_e\mu_N\langle(3\cos^2\theta-1)/r^3\rangle_S,\\
d &= (3/2)g_eg_N\mu_e\mu_N\langle\sin^2\theta/r^3\rangle_S,\\
eQq_1 &= eQ\langle(3\cos^2\theta-1)/r^3\rangle_T,\\
eQq_2 &= -3eQ\langle\sin^2\theta/r^3\rangle_T,
\end{aligned}
\tag{12}
$$

enable one to determine the electron distributions in IO $X\ ^2\Pi$. In Eq. (12) L refers to the electrons responsible for the orbital angular momentum, S denotes those electrons responsible for the molecular spin, and T includes all electrons. Equation (12) defines the hyperfine constants as average values for a single $^2\Pi$ state, implicitly assuming that these constants have identical values for both the X_1 and X_2 states. Although this assumption probably becomes less valid as the spin-orbit coupling increases, it is not possible to determine changes in the individual magnetic hyperfine constants experimentally. Thus, the a reported here is actually

$$
a = \tfrac{1}{2}(\langle X_1|h_+|X_1\rangle + \langle X_2|h_-|X_2\rangle), \tag{13}
$$

TABLE IX. Parameters derived from the magnetic hyperfine constants. r^{-3} and $\psi^2(0)$ in 10^{30} m^{-3}. Unpaired electron density ρ in %.

Parameter	IO	I atom [a]	ρ [a]	I atom [b]	ρ [b]
$\langle r^{-3}\rangle_S$	61.56	162.80	37.8	162.31	37.9
$\langle r^{-3}\rangle_L$	48.70	122.16	39.9	122.74	39.7
$\langle\psi^2(0)\rangle$	−0.716	−1.72		−1.72	
$\langle\sin^2\theta\rangle$	0.7612				

[a]Atomic iodine values taken from the relativistic Hartree-Fock (HF) calculations in Table 17 of Ref. 41.

[b]Atomic iodine values taken from the relativistic Dirac–Fock calculations in Table A.2 of Ref. 42.

where $h_\pm = a \pm \frac{1}{2}(b_F + 2c/3)$. Similarly, b_F and c are determined from the expectation values of $h_\pm$ as well as the matrix element $\langle X_1|b_F - c/3|X_2\rangle$. The magnetic constant d produces significant effects only in the X_2 state.

Table IX compares the IO molecular expectation values $\langle r^{-3}\rangle_L$ derived from a and $\langle r^{-3}\rangle_S$ derived from $d+c/3$ with those determined for atomic iodine from relativistic calculations.[40,41] Using the appropriate atomic iodine relativistic expectation values yields an unpaired electron density of 38–40% on the I atom, with the unpaired electron densities derived from $\langle r^{-3}\rangle_S$ only slightly less than those derived from $\langle r^{-3}\rangle_L$. The distribution of the unpaired electron in IO is consistent with the periodic trend observed for ClO (Ref. 24) and BrO (Ref. 24), $\rho_S(\mathrm{ClO})=0.35$, $\rho_S(\mathrm{BrO}) = 0.37$ with little difference between $\langle r^{-3}\rangle_L$ and $\langle r^{-3}\rangle_S$. We note that failing to distinguish between the atomic $\langle r^{-3}\rangle_L$ and $\langle r^{-3}\rangle_S$ expectation values will lead to a substantial difference between the unpaired electron density calculated from a and $d+c/3$. If, for example, the single atomic I value $\langle r^{-3}\rangle = 127.7\times10^{30}$ m^{-3} tabulated by Morton and Preston[42] is used, the unpaired electron density calculated from a, 38.1%, is consistent with that found for ClO and BrO, but the density of 48.2% calculated from $d+c/3$ is considerably higher.

The angular distribution of the unpaired spin about the I atom may be determined from $\langle\sin^2\theta\rangle = 2d/(3d+c)$. The value of 0.7611 indicates a slightly compressed p orbital. This is consistent with the trend seen in FO, ClO, and BrO of 0.8390,[43] 0.8146,[24] and 0.8003.[19] Although all of these values are close to the 0.8 expected of a p orbital, they indicate a possible problem in determining spin densities when only $\langle(3\cos^2\theta-1)r^{-3}\rangle_S$ is determinable. For example, in the case of the $^3\Sigma$ nitrogen monohalides, it is necessary to make an assumption about the angular distribution for both atoms. Usually one assumes that $\langle 3\cos^2\theta-1\rangle_S = -0.4$ as is the case for an atomic p orbital.[37] However, the range for the halogen monoxides is −0.517 for FO to −0.283 for IO.

The negative Fermi contact term, $b_F = -95.8(37)$ MHz, represents another interesting manifestation of relativistic effects in IO. Equation (12) indicates that b_F is defined by the product of several positive physical constants and the electron density at the iodine nucleus, $\langle\psi^2(0)\rangle_S$. Negative $\langle\psi^2(0)\rangle_S$ values have traditionally been attributed to spin polarization,[37] although one may also explain this behavior as a result of relativistic effects. In the absence of other effects, the unpaired p electron should contribute about −87 MHz to b_F. No s character can be attributed to the unpaired electron. For comparison, Sakamaki *et al.*[37] found $b_F = -61.75$ MHz for NI, a molecule in which the determination of the Fermi contact term is more direct. It is interesting that $b_F(\mathrm{NI})/b_F(\mathrm{IO}) = 0.645(25)$ and $c(\mathrm{NI})/c(\mathrm{IO}) = 0.683(13)$.

The value $C_I = 77.41(94)$ kHz reported in Table VIII represents the average of the nuclear spin-rotation constants for the X_1 and X_2 states. The neglected centrifugal distortion on a contaminates the value of C_I determined here, lowering it by perhaps a few kHz, but does not affect the interpretation of C_I. Within experimental error, C_I of an NX

molecule [35–37] is the same as that of the corresponding XO molecule.

The difference in the nuclear spin-rotation constants for the X_1 and X_2 states is related to the Fermi contact term b_F via

$$\Delta C_I = C_I(X_1) - C_I(X_2) = \frac{2(B-\gamma/2)(b_F - c/3)}{E(X_2)-E(X_1)}. \quad (14)$$

Solving Eq. (14) yields $\Delta C_I = 14.5$ kHz. This value is an order of magnitude smaller than the ΔC_I calculated for BrO,[19] due in part to the fact that $b_F - c/3 = 43$ MHz for IO or almost a factor 4 smaller than for BrO. Since the quantity $b + 2c/3$ is well determined, Eq. (14) indicates that every kHz change in ΔC_I that may be due to other causes contributes ≈ 2 MHz to the effective value of b_F.

The assumption that all the difference in the nuclear spin-rotation constant is due to the term on the left-hand side of Eq. (14) directly affects the value of $\langle \sin^2\theta \rangle$ derived from the magnetic hyperfine constants. In fact an equally good fit can be obtained with the assumption that $\langle \sin^2\theta \rangle = 0.8$ and that $c = -d/2$. This gives $b_F = -0.31(18)$, which is what one might expect in the absence of relativistic or spin-polarization effects. However, the difference in nuclear spin-rotation constants then becomes large with $C_I(X_1) = 53.34$ kHz and $C_I(X_2) = 101.54$ kHz. Because of this, and the fact that the values of both $\langle \sin^2\theta \rangle$ and b_F are consistent with the trends observed for the XO molecules, the assumption implicit in Eq. (14) seems the better choice. Nevertheless, there is an indeterminacy that cannot be removed by isotope effects and that must be kept in mind when comparing these parameters with results of *ab initio* calculations.

The vibrational changes of the hyperfine constants are consistent with the unpaired electron density gradually moving to oxygen atom and the single bond becoming less ionic as the atoms separate.

The quadrupole coupling constants reported in Table VIII include both the axial and nonaxial components, eQq_1 and eQq_2, respectively. In contrast to the magnetic hyperfine parameters, changes in eQq_1 between the X_1 and X_2 states may be determined from the experimental data. The axial quadrupole coupling was thus fitted using eQq_1 as the average $^2\Pi$ value and eQq_S as the difference $eQq_1(X_1) - eQq_1(X_2)$. The linear vibrational dependence was included in the fit for both eQq_1 and eQq_S. The fit also required a centrifugal distortion term for eQq_1. The derived quadrupole constants for the two states are also included in Table VIII to illustrate that, as is the case for the magnetic constants, the parameters describing the X_1 state are more precise. The nonaxial quadrupole constant eQq_2 is determined primarily from the splitting of the Λ doublets. Although eQq_2 is large, its contribution is of the order of the Λ doubling on the X_2 state[44] and is largest for the weak $\Delta F = 0$ transitions. The largest eQq_2 contributions to splittings observed in this work are approximately 5 MHz. The sign convention for the nonaxial term eQq_2 is that of Endo *et al.*[45]

The change in eQq_1 with electronic state may be attributable to several causes. As the spin-orbit coupling becomes larger, the $\Omega = 1/2$ and $\Omega = 3/2$ states mix with other states of the same Ω. In the limit of large spin-orbit coupling, Hund's case (c), the quantum numbers Λ and Σ are not well defined and only the quantum number Ω identifies individual electronic states. This would explain differences in the quadrupole couplings for $X_1\ ^2\Pi_{3/2}$ and $X_2\ ^2\Pi_{1/2}$ even though IO is best considered as a case (a) molecule.

A potentially important difference in quadrupole coupling between the $X_1$and X_2 states comes from a relativistic contribution. The electric field gradient at the nucleus due to a p electron is a function of two radial integrals[40,46] and has been described previously.[19] If the two states have no other differences and an unpaired electron density ρ_s on the halogen, then Eq. (15) defines the relativistic contribution to eQq_S in terms of correction factors tabulated by Pyykkö and Seth[46] and the atomic quadrupole coupling constant for the $5p_{3/2}$ electron:[47]

$$eQq_S^{\mathrm{rel}} = \frac{2\rho_s(C_{+-} - C_{++})(eQq_{n10})}{3C_{++}}. \quad (15)$$

For IO the relativistic contribution corresponds to 81.4 MHz. It should be mentioned that Eq. (15) refers to the quasirelativistic limit.[46]

Structural differences between the X_1 and X_2 states also contribute to eQq_S since the different r_e values in the two states produce different electron distributions and electric field gradients at the iodine nucleus. One may estimate the amount that the bond length change contributes to eQq_S using Eq. (16):

$$eQq_S^{\mathrm{struct}} = eQq_{1_{10}}\frac{A_{01}}{Y_{11}}. \quad (16)$$

For IO the structural contribution to eQq_S equals 38.5 MHz. The total calculated value for eQq_S is thus 119.1 MHz. This is the correct sign and order of magnitude as the fitted value $eQq_S = 198.17(65)$ MHz but underestimates the experimental result by 40%. Although the difference of about 79 MHz is not large compared to the total quadrupole coupling constant, it is apparent that the simple approximation of relativistic effects worsens as one proceeds from ClO to IO and that there may be small changes in electronic structure. This is not surprising in view of the considerable increase in spin-orbit coupling. A more detailed description of the quadrupole coupling changes would involve a determination of the mixing of the $X_1\ ^2\Pi_{3/2}$ and $X_2\ ^2\Pi_{1/2}$ states with other states as mentioned above.

These differences in electronic structure due to mixing may also affect the magnetic hyperfine parameters (see above), but the effects are not independently determinable. The definitions of the magnetic hyperfine constants used to derive the unpaired electron density are not rigorously correct since there is the implicit assumption that the electron distribution is the same in the $X_1\ ^2\Pi_{3/2}$ and $X_2\ ^2\Pi_{1/2}$ states. Nevertheless, the derived unpaired electron densities are consistent with what one should expect for IO, provided the relativistically corrected atomic iodine radial integrals are used in the derivation. Finally, the derived angular distribution is consistent with a predominantly $p(\pi)$ electron on the iodine atom.

The nonaxial quadrupole coupling constant eQq_2 results from a noncylindrical distribution of electron density about the molecular axis. In the case of the halogen oxides, the asymmetry is attributed to the vacancy in the $p(\pi^*)$ orbital containing the unpaired electron. It is, therefore, useful to compare the unpaired electron density derived from eQq_2 with those derived from the spin and orbital magnetic constants. As has been discussed above, the quantity referred to as $\langle r^{-3}\rangle_T$ is different for a $p(\pi_{1/2})$ from that of a $p(\pi_{3/2})$ electron. For eQq_2 we shall use the relativistic correction factor for the average of the two $p(\pi)$ orbitals from Ref. 46. If one then uses the angular distribution derived from the magnetic constants, the calculated unpaired electron density on the halogen is 35%, 36%, and 44% for ClO, BrO, and IO, respectively. For the two lighter monoxides, the agreement with densities derived from the magnetic constants is very good. For IO the density derived from eQq_2 is somewhat higher, but it is clear that the dominant contribution is from the vacancy in the $p(\pi^*)$ orbital containing the electron that gives rise to the magnetic constants.

CONCLUSION

The pure rotational spectrum of the IO radical has been analyzed using a set of isotopically independent parameters. Predictions of transitions based on the data reported here may be used for submillimeter and far-infrared atmospheric remote sensing measurements. The parameters describe states that have not been previously observed at high resolution and can provide the basis for assignment of rotationally resolved IO spectra in other spectral regions. The extensive data from vibrationally excited states have yielded RKR potentials for internal IO energies up to 8000 cm^{-1}, which have been compared to recent *ab initio* calculations. The inclusion of transitions from both the $X_1\ ^2\Pi_{3/2}$ and $X_2\ ^2\Pi_{1/2}$ states as well as $^{127}I^{18}O$ transitions allowed the determination of a complete set of hyperfine constants and the decorrelation of the electron spin-rotation constant γ from A_{01}. The fitted hyperfine constants have been compared with atomic values derived from relativistic calculations to provide information on the electron distribution in the molecule. Although there is probably some difference in the distribution of the electrons in the $X_1\ ^2\Pi_{3/2}$ and $X_2\ ^2\Pi_{1/2}$ states, interpretation of the hyperfine constants suggests that the difference is not large. It is hoped that the molecular constants reported here will serve as benchmarks for future relativistic *ab initio* calculations.

ACKNOWLEDGMENTS

The authors thank A. Alekseyev for the IO *ab initio* energy data and insightful comments regarding the calculations. They also acknowledge useful comments from P. Pyykkö. This paper presents research carried out at the Jet Propulsion Laboratory, California Institute of Technology, under contract with the National Aeronautics and Space Administration.

[1] R. P. Wayne, G. Poulet, P. Biggs *et al.*, Atmos. Environ. **29**, 2677 (1995).
[2] S. Solomon, R. R. Garcia, and A. R. Ravishankara, J. Geophys. Res. **99**, 20491 (1994).
[3] I. Pundt, J.-P. Pommerau, C. Phillips, and E. Lateltin, J. Atmos. Chem. **30**, 173 (1996).
[4] P. O. Wennberg, J. W. Brault, T. F. Hanisco, R. J. Salawitch, and G. H. Mount, J. Geophys. Res. **102**, 8887 (1997).
[5] J. Stotz, K. Herbstreit, B. Alicke, and U. Platt, J. Atmos. Chem. **34**, 65 (1999).
[6] B. Alicke, K. Herbstreit, J. Stotz, and U. Platt, Nature (London) **397**, 572 (1999).
[7] F. Wittrock, R. Müller, A. Richter, H. Bovensmann, and J. P. Burrows, Geophys. Res. Lett. **27**, 1471 (2000).
[8] R. A. Durie and D. A. Ramsay, Can. J. Phys. **36**, 35 (1958).
[9] R. A. Durie, F. Legay, and D. A. Ramsay, Can. J. Phys. **38**, 444 (1960).
[10] J. P. Bekooy, W. L. Meerts, and A. Dymanus, J. Mol. Spectrosc. **102**, 320 (1983).
[11] S. M. Newman, W. H. Howie, I. C. Lane, M. R. Upson, and A. J. Orr-Ewing, J. Chem. Soc., Faraday Trans. **94**, 2681 (1998).
[12] A. Carrington, P. N. Dyer, and D. H. Levy, J. Chem. Phys. **52**, 309 (1970).
[13] J. M. Brown, C. R. Byfleet, B. J. Howard, and D. K. Russell, Mol. Phys. **23**, 457 (1972).
[14] C. R. Byfleet, A. Carrington, and D. K. Russell, Mol. Phys. **20**, 271 (1971).
[15] S. Saito, J. Mol. Spectrosc. **48**, 530 (1973).
[16] M. K. Gilles, M. L. Polak, and W. C. Lineberger, J. Chem. Phys. **95**, 4723 (1991).
[17] F. Tamassia, S. M. Kermode, and J. M. Brown, J. Mol. Spectrosc. **205**, 92 (2001).
[18] H. S. P. Müller, C. E. Miller, and E. A. Cohen, J. Chem. Phys. **107**, 8292 (1997).
[19] B. J. Drouin, C. E. Miller, H. S. P. Müller, and E. A. Cohen, J. Mol. Spectrosc. **205**, 128 (2001).
[20] C. E. Miller and E. A. Cohen, International Symposium on Molecular Spectroscopy, Abstract TJ07, Columbus, OH, 1999.
[21] H. M. Pickett, J. Mol. Spectrosc. **148**, 371 (1991).
[22] See E-PAPS Document No. E-JCPSA6-115-008137 for observed frequencies used in the final fit, uncertainties, assignments, residuals, and extended precision parameters. This document may be retrieved via the EPAPS homepage (http://www.aip.org/pubservs//epaps.html) or from ftp.aip.org in the directory /epaps/. See the EPAPS homepage for more information.
[23] J. M. Brown, E. A. Colbourn, J. K. G. Watson, and F. D. Wayne, J. Mol. Spectrosc. **74**, 294 (1979).
[24] B. J. Drouin, C. E. Miller, E. A. Cohen, G. Wagner, and M. Birk, J. Mol. Spectrosc. **207**, 4 (2001).
[25] C. E. Miller and B. J. Drouin, J. Mol. Spectrosc. **205**, 312 (2001).
[26] G. Audi and A. H. Wapstra, Nucl. Phys. A **595**, 409 (1995).
[27] H. M. Pickett, R. L. Poynter, E. A. Cohen, M. L. Delitsky, J. C. Pearson, and H. S. P. Müller, J. Quant. Spectrosc. Radiat. Transf. **60**, 883 (1998).
[28] R. J. Le Roy, J. Mol. Spectrosc. **194**, 189 (1999).
[29] J. K. G. Watson, J. Mol. Spectrosc. **45**, 99 (1973).
[30] J. M. Brown and J. K. G. Watson, J. Mol. Spectrosc. **65**, 65 (1977).
[31] J. L. Dunham, Phys. Rev. **41**, 721 (1932).
[32] J. P. Bouanich, J. Quant. Spectrosc. Radiat. Transf. **19**, 381 (1978).
[33] R. J. Le Roy, University of Waterloo Chemical Physics Report CP-425, 1992. See also http://leroy.uwaterloo.ca
[34] S. Roszak, M. Krauss, A. B. Alekseyev, H.-P. Liebermann, and R. J. Buenker, J. Phys. Chem. A **104**, 2999 (2000); A. B. Alekseyev (personal communication).
[35] C. Yamada, Y. Endo, and E. Hirota, J. Chem. Phys. **79**, 4159 (1983).
[36] T. Sakamaki, T. Okabayashi, and M. Tanimoto, J. Chem. Phys. **109**, 7169 (1998).
[37] T. Sakamaki, T. Okabayashi, and M. Tanimoto, J. Chem. Phys. **111**, 6345 (1999).
[38] M. K. Gilles, M. L. Polak, and W. C. Lineberger, J. Chem. Phys. **96**, 8012 (1992).
[39] R. S. Mulliken and A. Christy, Phys. Rev. **38**, 87 (1931).
[40] I. Lindgren and A. Rosén, Case Stud. At. Phys. **4**, 197 (1974). In Table 17 $\langle r^{-3}\rangle_L = \langle r^{-3}\rangle_{01}$ and $\langle r^{-3}\rangle_S = \langle r^{-3}\rangle_{12}$. The expectation values in Table 17 require a factor of a_0^{-3} to convert them into SI units.
[41] P. Pyykkö and L. Wiesenfeld, Mol. Phys. **43**, 557 (1981). The hyperfine integrals from Table A2 are related to the R_{++}, R_{+-}, and R_{--} terms from Ref. 41: $V(1)=2R_{--}$, $V(1,-2)=R_{+-}/2$ and $V(-2)=-R_{++}$.

The atomic iodine expectation values are then determined from the relationships $\langle r^{-3}\rangle_L = \frac{1}{9}[4R_{++} + 4R_{--} - R_{+-}]$ and $\langle r^{-3}\rangle_S = \frac{1}{27}[-8R_{++} + 40R_{--} - 5R_{+-}]$. The numerical results require a factor of $a_0^{-3}\alpha^{-1}$ to convert them into SI units.

[42] J. R. Morton and K. F. Preston, J. Magn. Reson. (1969-1992) **30**, 577 (1978).

[43] F. Tamassia, J. M. Brown, and K. M. Evenson, J. Chem. Phys. **110**, 7273 (1999).

[44] E. A. Cohen, H. M. Pickett, M. Geller, J. Mol. Spectrosc. **87**, 459 (1981).

[45] Y. Endo, S. Saito, and E. Hirota, J. Mol. Spectrosc. **94**, 199 (1982).

[46] P. Pyykkö and M. Seth, Theor. Chem. Acc. **96**, 92 (1997).

[47] H. H. Brown and J. G. King, Phys. Rev. **142**, 53 (1966).